

A three-constituent damage model for arterial clamping in computer-assisted surgery

Nele Famaey · Jos Vander Sloten · Ellen Kuhl

Received: date / Accepted: date

Abstract Robotic surgery is an attractive, minimally invasive and high precision alternative to conventional surgical procedures. However, it lacks the natural touch and force feedback that allows the surgeon to control safe tissue manipulation. This is an important problem in standard surgical procedures such as clamping, which might induce severe tissue damage. In complex, heterogeneous, large deformation scenarios, the limits of the safe loading regime beyond which tissue damage occurs are unknown. Here, we show that a continuum damage model for arteries, implemented in a finite element setting, can help to predict arterial stiffness degradation and to identify critical loading regimes.

The model consists of the main mechanical constituents of arterial tissue: extracellular matrix, collagen fibres, and smooth muscle cells. All constituents are allowed to degrade independently in response to mechanical overload. To demonstrate the modularity and portability of the proposed model, we implement it in a commercial finite element program, which allows to keep track of damage progression via internal variables.

The loading history during arterial clamping is simulated through four successive steps, incorporating residual strains. The results of our first prototype simulation demonstrate significant regional variations in smooth muscle cell damage. In three additional steps, this damage is evaluated by simulating an isometric contraction experiment. The entire finite element simulation is finally compared to actual *in vivo* experiments.

In the short term, our computational simulation tool can be useful to optimize surgical tools with the goal to

minimize tissue damage. In the long term, it can potentially be used to inform computer-assisted surgery, and identify safe loading regimes, in real time, to minimize tissue damage during robotic tissue manipulation.

Keywords artery · damage · smooth muscle cells · active contraction · residual stress · finite elements

1 Introduction

For the past two decades, computer-assisted surgery has revolutionised surgical treatment in various different fields. Initially developed to surgically manipulate the brain, see Kwok et al. [1988], robotic surgery has now gained widespread use. The da Vinci surgical system, for example, offers a computer-enhanced surgical option for complex cardiovascular procedures, see Mohr et al. [2001]. Robotic surgery enables minimally invasive and high precision treatment. However, in contrast to conventional surgeries, robotic surgery inherently lacks the natural touch and force feedback. This is an important problem during common surgical procedures such as grasping, cutting, stapling, clipping, and clamping, which may induce severe tissue damage when not controlled appropriately.

To illustrate these effects, within this manuscript, we focus in particular on arterial clamping, which always entails a certain degree of undesired iatrogenic tissue damage [Barone et al., 1989]. Research has been directed towards decreasing this unnecessary intraoperative trauma, for example through the design of less traumatic surgical instruments [Gupta et al., 1997]. Obviously, the effectiveness of these new designs and techniques depends on how well damage mechanisms are understood and how accurately thresholds for safe

N. Famaey
Celestijnenlaan 300C, 3001 Leuven, Belgium
Tel.: +32-16-328981, Fax: +32-16-327994
E-mail: nele.famaey@mech.kuleuven.be

tissue loading can be defined.

An important aspect is the accurate modelling of the loading and the resulting damage process. This article describes a new material model for cardiovascular tissue, which is an extension of the Holzapfel-material model for arterial tissue [Holzapfel et al., 2000], incorporating smooth muscle cell activation according to Murtada et al. [2010] and damage according to Balzani et al. [2006]. The model is suitable to simulate the damage process during the clamping of an artery. It displays the decrease of active force generation in smooth muscle cells due to the sustained damage. Embedded in a finite element environment, this new model provides a useful tool to define safe loading regimes for arterial tissue, which could be used to inform computer-enhanced surgical systems to minimize tissue damage in robotic surgery and, in general, to optimize clamp design towards minimal trauma.

Physiology of the healthy artery

An artery consists of three distinct layers. In healthy arterial tissue, the inner layer, or intima, consists of an endothelial layer. The middle layer, the media, is the most important load-bearing layer of the artery within the physiological loading domain. It consists of collagen, elastin and smooth muscle cells separated by fenestrated elastic laminae. The outer layer, the adventitia, is surrounded by loose connective tissue. It consists mainly of thick bundles of collagen fibres arranged in a helical structure [Schriebl et al., 2011]. For a more detailed description of arterial wall morphology, the reader is referred to, for example, Rhodin [1979] and Holzapfel et al. [2000].

Arterial blood pressure is regulated acutely by altering the luminal diameter, which is controlled by balancing vasoconstricting and vasodilating influences on the smooth muscle cells in a mechanochemical process. Smooth muscle cells contain actin and myosin filaments that slide relative to each other, causing the contraction and relaxation. This relative sliding is accomplished by the configurational changes of the cross-bridges, or myosin heads, that connect the myosin to the actin filament. These configurational changes are caused by the phosphorylation and dephosphorylation of the myosin heads, as a function of the intracellular calcium concentration. For a detailed description of the mechanochemical process of smooth muscle cell contraction, the reader is referred to, for example, Stålhand et al. [2008] or Murtada et al. [2010].

Material modelling

Constitutive models characterize the mechanical behaviour of materials through a functional relation between stresses and strains. A great number of models for cardiovascular tissue exist, trying to capture its specific features [Vito and Dixon, 2003, Göktepe et al., 2011]. For an overview of constitutive models for cardiovascular tissue, or for biological soft tissue in general, the reader is referred to, for example, Gasser et al. [2006], Famaey and Vander Sloten [2008]. Holzapfel et al. [2000] have introduced one of the most commonly used hyperelastic, anisotropic material models for arteries, which accounts for two collagen fibre families along two symmetrically arranged directions and allows for a certain amount of dispersion. This model nicely captures the typical nonlinear behaviour as wavy collagen fibres are gradually recruited when the tissue is stretched. In this baseline model, however, the material behaves completely passive, i.e., the model does not account for the contractile nature of the smooth muscle cells present in the arterial wall.

The first mechanical representation of a muscle was proposed by Hill [1938], which was extended to the three-element Hill model by Fung [1970]. This model consists of a dashpot representing the contractile element in series with a spring element representing the contractile unit. Another spring in parallel represents the surrounding material. For smooth muscle, Gestrelius and Borgström [1986] proposed a variation of the three-element Hill model. Yang et al. [2003] were the first to couple the mechanical representation to an electrochemical model by Hai and Murphy [1988], incorporating the calcium-driven configurational changes of the cross-bridges. This approach was also followed and improved for situations with large deformations, by Stålhand et al. [2008], Murtada et al. [2010], Kroon [2010] and Schmitz and Böl [2011]. However, so far, the active contribution of smooth muscle has not yet been combined with the collagen fibre contribution, nor have the models been implemented in a finite element framework. The model proposed by Zulliger et al. [2004] does combine the active contribution with a stochastic collagen fibre contribution in a pseudoelastic-type strain-energy function. In Göktepe and Kuhl [2010] and Rausch et al. [2011] finite element formulations were proposed in which mechanical contraction was controlled via electrical and chemical fields, respectively. Unfortunately, these models are phenomenological and thus less straightforward to populate with realistic experiment-based material parameters. In this paper, the active contribution by Murtada et al. [2010] will be combined with the collagen fibre contribution

by Holzapfel et al. [2000] and implemented in a finite element framework to account for tissue heterogeneity. Moreover, the material parameters related to the active constituent will be calibrated by means of suitable experiments.

Most existing material models are designed to describe the material in its physiological state. These models, however, fail to capture damage mechanisms that may occur when the tissue is loaded in the sub- or supra-physiological domain, for example, during surgical manipulation. Motivated by the typical stress softening or Mullins effect in rubber-like materials, Simo and Ju [1987] introduced a discontinuous damage model that allows to capture progressive degradation of an isotropic material. Balzani et al. [2006] have adapted this approach to describe damage to arterial tissue based on the Holzapfel material model. Other approaches exist to model damage in rubber-like materials, in a continuous manner [Miehe, 1995], or pseudoelastically [Ogden and Roxburgh, 1999]. Hokanson and Yazdani [1997] incorporated anisotropic damage to arteries by weighting an Ogden-type strain energy function with a fourth order damage tensor. Also for arterial tissue, damage to the collagen fibres has been described in a stochastic, worm-like chain model by Rodríguez et al. [2006]. From the same group, Calvo et al. [2007] presented a continuum damage model with discontinuous softening in matrix and collagen fibres. Viscoelasticity was introduced in these damage models by Pena et al. [2010]. These damage models, however, neither include the active smooth muscle contribution nor the damage to the smooth muscle cells. In this paper, damage will be incorporated in analogy to Balzani et al. [2006], this time including the contributions of healthy and potentially damaged smooth muscle cells.

Experimental characterization

Every constitutive model introduces a set of material parameters that needs to be calibrated for the particular type of tissue. Specific experimental setups, such as uniaxial and biaxial tensile tests or extension-inflation tests can be performed to identify the material parameters for standard passive hyperelastic models, as described, for example, in Sacks and Sun [2003], Holzapfel and Ogden [2010].

To quantify the active response of the smooth muscle, isometric and/or isotonic contraction experiments can be performed *ex vivo*, as described in Barone et al. [1989], Gleason et al. [2004], Murtada et al. [2010] and Böl et al. [2011]. Recently, Itoh et al. [2009] and Tsamis et al. [2011] have reported *in vivo* experiments to identify active muscle force in cardiovascular tissue *in situ*.

Damage is frequently assessed through the evaluation of histological images of the tissue, for example in Hsi et al. [2002], Manchio et al. [2005] and De et al. [2007]. For example, live-dead stains can help to identify cell viability, and H&E (haematoxylin and eosine) and Caspase-3 stains can visualize ruptures in the collagen fibres. Unfortunately, most studies of tissue damage are qualitative in nature, both in the application of the tissue load to induce the damage and in the subsequent damage assessment. To identify the damage material parameters, however, quantitative experiments are essential. De et al. [2007] were the first to characterize damage quantitatively for porcine liver. For cardiovascular tissue, previous work [Famaey et al., 2010] reports on a study in which the damage to the smooth muscle cells of rat abdominal arteries is quantitatively assessed in an isometric contraction test after *in vivo* clamping to well-defined loading levels. In this article, this quantitative damage information will be used to identify the parameters of the new material model.

Outline

Section 2 introduces our new material model, accounting for the three major tissue constituents: extracellular matrix, collagen and smooth muscle cells. In particular, we allow each constituent to degrade independently. The features of the model are first illustrated in a simple homogeneous uniaxial cyclic extension test in section 3. Section 4 then demonstrates how the model can be applied to predict smooth muscle cell damage in rat abdominal arteries through clamping and how the damage parameters can be identified using actual experiments. Section 5 discusses the presented model and suggests further directions for future work.

2 Governing equations for arteries

Through an additive decomposition of the strain energy, the following constitutive model for active healthy and degraded arterial tissue characterises the properties of (i) an isotropic matrix material constituent, (ii) an anisotropic constituent attributed to the dispersed collagen fibres and (iii) an anisotropic smooth muscle cell constituent. The first two constituents are motivated by the Holzapfel-material model as proposed in Holzapfel et al. [2000], whereas the third component is motivated by the mechanical smooth-muscle-activation model described by Murtada et al. [2010]. The damage accumulating in the different constituents during mechanical loading is characterised through a strain-energy-driven damage function for each individual constituent, motivated by the formation by Balzani et al. [2006]. In the

remainder of the paper, the model will be referred to as the three-constituent damage model.

2.1 Kinematic prerequisites

Since soft biological tissues can undergo large physiological deformations, the key kinematic quantity to characterize the deformation process is the deformation gradient \mathbf{F} , i.e., the gradient of the deformation map φ with respect to the undeformed position \mathbf{X} :

$$\mathbf{F} = \nabla_{\mathbf{X}} \varphi \quad \text{and} \quad J = \det(\mathbf{F}). \quad (1)$$

Here, J denotes its Jacobian J , which is close to one, $J \approx 1$, for nearly incompressible materials. In that case, it proves convenient to decompose the deformation gradient into a deviatoric part, $\bar{\mathbf{F}}$, and a volumetric part, $J^{1/3}\mathbf{I}$,

$$\mathbf{F} = J^{1/3}\bar{\mathbf{F}}. \quad (2)$$

Typically, the deformation of incompressible materials is characterised in terms of the invariants of the deviatoric part $\bar{\mathbf{C}}$ of the right Cauchy-Green tensor \mathbf{C} , with

$$\mathbf{C} = \mathbf{F}^T \mathbf{F} \quad \text{and} \quad \bar{\mathbf{C}} = \bar{\mathbf{F}}^T \bar{\mathbf{F}}. \quad (3)$$

The basic deviatoric invariants I_i take the following explicit representation:

$$\begin{aligned} I_1 &= \text{tr}(\bar{\mathbf{C}}), \\ I_2 &= \frac{1}{2} [\text{tr}^2(\bar{\mathbf{C}}) - \text{tr}(\bar{\mathbf{C}}^2)], \\ I_3 &= \det(\bar{\mathbf{C}}). \end{aligned} \quad (4)$$

While the basic invariants characterize the isotropic material behaviour, the anisotropic invariants I_4^{fib} , I_6^{fib} , and I_4^{smc} characterize the stretches along the fibre and smooth muscle cell directions, see [Gasser et al., 2006]:

$$\begin{aligned} I_4^{\text{fib}} &= \lambda_\theta^2 \cos^2 \alpha^{\text{fib}} + \lambda_z^2 \sin^2 \alpha^{\text{fib}}, \\ I_6^{\text{fib}} &= \lambda_\theta^2 \cos^2 \alpha^{\text{fib}} + \lambda_z^2 \sin^2 \alpha^{\text{fib}}, \\ I_4^{\text{smc}} &= \lambda_\theta^2 \cos^2 \alpha^{\text{smc}} + \lambda_z^2 \sin^2 \alpha^{\text{smc}} \end{aligned} \quad (5)$$

Here, λ_θ and λ_z are the stretches in the circumferential and axial directions, respectively. Moreover, α^{fib} and α^{smc} denote the angles between the circumference and the mean directions of the fibre and smooth muscle families. In the case of arteries, two fibre families are oriented symmetrically with respect to the cylinder axis, so that $I_4 = I_6$. Finally, the pseudo-invariants $I_4^{\text{fib}\star}$ and $I_6^{\text{fib}\star}$ are introduced to account for dispersion,

$$\begin{aligned} I_4^{\text{fib}\star} &= \kappa I_1 + [1 - 3\kappa] I_4^{\text{fib}}, \\ I_6^{\text{fib}\star} &= \kappa I_1 + [1 - 3\kappa] I_6^{\text{fib}}, \end{aligned} \quad (6)$$

where the fibre dispersion κ characterises the degree of anisotropy varying from $\kappa = 0$ in the anisotropic non-disperse state to $\kappa = \frac{1}{3}$ in the isotropic state.

2.2 Constitutive equations

Since the tissue is assumed to be nearly incompressible, it is common to additively decompose the strain-energy function Ψ ,

$$\Psi = \Psi^{\text{vol}} + \Psi^{\text{dev}} = \Psi^{\text{vol}} + \Psi^{\text{mat}} + \Psi^{\text{fib}_4} + \Psi^{\text{fib}_6} + \Psi^{\text{smc}}, \quad (7)$$

into a volumetric Ψ^{vol} and a deviatoric Ψ^{dev} part. The latter consists of an isotropic contribution of the matrix material Ψ^{mat} , an anisotropic contribution of two families of collagen fibres Ψ^{fib_4} and Ψ^{fib_6} , and a contribution of the smooth muscle cells Ψ^{smc} . The individual contributions will be specified in detail in the sequel. All deviatoric components are allowed to undergo degradation in the case of physiological overload. Simo and Ju [1987] in general and Balzani et al. [2006] for arteries have described the approach of weighting the strain energy with a scalar valued damage variable $[1 - d]$. This model builds upon the classical damage concept, and introduces an independent damage variable for each individual constituent.

Volumetric bulk material

The volumetric free energy Ψ^{vol} can, for example, be expressed as follows:

$$\Psi^{\text{vol}} = \Lambda \left[\frac{1}{2} [J^2 - 1] - \ln(J) \right]. \quad (8)$$

The penalty parameter Λ is chosen to $\Lambda = 5.0$ after a sensitivity analysis demonstrating that this value was low enough to ensure near-incompressibility. Since this term is handled separately in an incompressible finite element formulation, we will now focus on the four contributions to the deviatoric energy Ψ^{dev} , which are the primary descriptors of the material behaviour.

Extracellular matrix

The extracellular matrix is characterised through an isotropic free energy Ψ^{mat} , which is allowed to degrade according to the classical damage concept:

$$\Psi^{\text{mat}} = [1 - d^{\text{mat}}] \hat{\Psi}^{\text{mat}}. \quad (9)$$

Here, $\hat{\Psi}^{\text{mat}}$ denotes the elastic energy of the extracellular matrix:

$$\hat{\Psi}^{\text{mat}} = \frac{1}{2} c [I_1 - 3], \quad (10)$$

where $c > 0$ characterises the matrix stiffness. The evolution of the damage variable of the extracellular matrix d^{mat} is driven by the undamaged elastic extracellular matrix energy:

$$d^{\text{mat}} = \gamma^{\text{mat}} [1 - \exp(-\beta^{\text{mat}}/m^{\text{mat}})]. \quad (11)$$

The weighting factor γ^{mat} can be used to turn damage on, $\gamma^{\text{mat}} \in]0, 1]$, or off, $\gamma^{\text{mat}} = 0$, and m^{mat} is a parameter of the damage model. The variable β^{mat} is an internal variable keeping track of the maximum elastic strain energy experienced so far, within the time interval $0 \leq t \leq \tau$:

$$\beta^{\text{mat}} = \max_{0 \leq t \leq \tau} (\widehat{\Psi}^{\text{mat}}(t) - \Psi_0^{\text{mat}}). \quad (12)$$

Since it can be assumed that no damage occurs in the physiological range, the damage threshold Ψ_0^{mat} is initialised with the strain energy in the extracellular matrix at systolic pressure. For heterogeneous problems, Ψ_0^{mat} may therefore differ for each material point, and is thus not strictly a material property.

Collagen fibres

Collagen fibres will only contribute when under tension. Similar to the free energy of the matrix, the free energy of the collagen fibres accounts for both an elastic and a degrading response,

$$\Psi^{\text{fbi}} = [1 - d^{\text{fbi}}] \widehat{\Psi}^{\text{fbi}} \quad i = 4, 6, \quad (13)$$

where the energy contributions of the two families of collagen fibres are formulated according to Holzapfel et al. [2000]:

$$\widehat{\Psi}_{\text{fbi}} = \frac{k_1}{2k_2} \exp(k_2 [I_i^* - 1]^2) - 1. \quad (14)$$

Here, $k_1 > 0$ characterises the fibre stiffness and $k_2 > 0$ is a dimensionless parameter. Damage of the two fibre families d^{fbi} can again be described in terms of the elastic fibre energies $\widehat{\Psi}^{\text{fbi}}$:

$$d^{\text{fbi}} = \gamma^{\text{fb}} [1 - \exp(-\beta^{\text{fbi}}/m^{\text{fb}})], \quad (15)$$

where γ^{fb} and m^{fb} are the two fibre damage parameters and β^{fbi} are the internal variables of each fibre family keeping track of the maximum value of the elastic fibre energies experienced so far:

$$\beta^{\text{fbi}} = \max_{0 \leq t \leq \tau} (\widehat{\Psi}^{\text{fbi}}(t) - \Psi_0^{\text{fb}}). \quad (16)$$

Again, the damage threshold Ψ_0^{fb} is initialised with the strain energy of the fibres at systolic pressure, and may therefore differ for each material point. Since the internal variables β^{fbi} are driven by the elastic strain energies $\widehat{\Psi}^{\text{fbi}}$, material degradation will only take place when the fibres are under tension, as the strain energy is zero when in compression.

Smooth muscle cells

The smooth muscle cells form an integral part of the

matrix constituent, even in their passive state. Therefore, their degradation is assumed to depend on both the passive damage $d_{\text{pas}}^{\text{smc}}$ in the surrounding matrix and the active damage $d_{\text{pas}}^{\text{smc}}$ in the smooth muscle cells themselves:

$$\Psi^{\text{smc}} = [1 - d_{\text{pas}}^{\text{smc}}][1 - d_{\text{act}}^{\text{smc}}] \widehat{\Psi}^{\text{smc}}. \quad (17)$$

In the undamaged state, the energy of the smooth muscle cells $\widehat{\Psi}^{\text{smc}}$ can be expressed as follows:

$$\widehat{\Psi}^{\text{smc}} = \frac{1}{2} \mu^{\text{smc}} [n_{\text{III}} + n_{\text{IV}}][\sqrt{I_4^{\text{smc}}} + u_{\text{rs}} - 1]^2, \quad (18)$$

where μ^{smc} characterises the stiffness of the actin-myosin filament apparatus. The kinetics of the actin-myosin powerstroke are modelled through a four-state model described by Hai and Murphy [1988] and adopted by Murtada et al. [2010], Kroon [2010] and Stålhand et al. [2011]. This model describes the transitions between the four states n_{I} , n_{II} , n_{III} and n_{IV} of the myosin heads as a function of the calcium concentration as follows:

$$\begin{bmatrix} \dot{n}_{\text{I}} \\ \dot{n}_{\text{II}} \\ \dot{n}_{\text{III}} \\ \dot{n}_{\text{IV}} \end{bmatrix} = \begin{bmatrix} -\kappa_1 & \kappa_2 & 0 & \kappa_7 \\ \kappa_1 & -(\kappa_2 + \kappa_3) & \kappa_4 & 0 \\ 0 & \kappa_3 & -(\kappa_4 + \kappa_5) & \kappa_6 \\ 0 & 0 & \kappa_5 & -(\kappa_6 + \kappa_7) \end{bmatrix} \begin{bmatrix} n_{\text{I}} \\ n_{\text{II}} \\ n_{\text{III}} \\ n_{\text{IV}} \end{bmatrix} \quad (19)$$

Here, n are the fractions of the four states, which sum up to one, $\sum n_i = 1$. The κ_i are the rate constants of the model, where κ_1 and κ_7 are a function of the calcium concentration. In particular, n_{I} and n_{II} , are the fractions of dephosphorylated and phosphorylated myosin heads that are not attached to the actin filament, and thus not mechanically contributing. n_{III} and n_{IV} are the fractions of phosphorylated and dephosphorylated myosin heads, or cross-bridges, attached to the actin filaments, and thus contributing to the stiffness. The power-stroke occurs through a conformational change in state III, after which the myosin heads transform back into state II. As long as the myosin heads remain phosphorylated, they cycle back and forth between states II and III, thus generating contraction. In state IV, the myosin heads are still attached to the actin filament but dephosphorylated and thus unable to perform a power stroke.

In equation (18), u_{rs} is the average normalised relative sliding between the myosin and the actin filaments. It follows a viscous evolution law:

$$\dot{u}_{\text{rs}} = \frac{1}{\eta} [P^{\text{smc}} - P^{\text{mat}}], \quad (20)$$

where η is a viscosity parameter, P^{smc} denotes the active stress exerted by the attached myosin heads and P^{mat} denotes the stress from the surrounding matrix.

The active stress P^{smc} can be approximated by the following step function:

$$P^{\text{smc}} = \begin{cases} \kappa_c n_{\text{III}} & \text{for } P^{\text{mat}} < \kappa_c n_{\text{III}} \\ P^{\text{mat}} & \text{else} \\ \kappa_c [n_{\text{III}} + n_{\text{IV}}] & \text{for } \kappa_c [n_{\text{III}} + n_{\text{IV}}] < P^{\text{mat}}, \end{cases} \quad (21)$$

where κ_c is a material parameter related to the driving force per myosin head, see Murtada et al. [2010] and Kroon [2010] for details. Smooth muscle cell degradation is governed by two damage variables, $d_{\text{pas}}^{\text{smc}}$ characterizing the damage to the surrounding matrix and $d_{\text{act}}^{\text{smc}}$ characterizing the damage to the smooth muscle cells themselves:

$$\begin{aligned} d_{\text{pas}}^{\text{smc}} &= \gamma_{\text{pas}}^{\text{smc}} [1 - \exp(-\beta^{\text{mat}}/m_{\text{pas}}^{\text{smc}})], \\ d_{\text{act}}^{\text{smc}} &= \gamma_{\text{act}}^{\text{smc}} [1 - \exp(-\beta^{\text{smc}}/m_{\text{act}}^{\text{smc}})]. \end{aligned} \quad (22)$$

The internal variable for matrix damage β^{mat} is defined in equation (12), and the internal variable for smooth muscle cell damage β^{smc} is defined as:

$$\beta^{\text{smc}} = \max_{0 \leq t \leq \tau} (\hat{\Psi}^{\text{smc}}(t) - \Psi_0^{\text{smc}}). \quad (23)$$

Both keep track of the loading history through the maximum value of the elastic matrix and smooth muscle cell energies experienced so far.

3 Computational modeling of arteries

This section addresses the implementation of the arterial model into the finite element program Abaqus.

3.1 Implementation

The constitutive model is implemented in the Abaqus user subroutine UANISOHYPER_INV, a family of subroutines designed for anisotropic, hyperelastic material models, in which the strain energy density function Ψ is formulated as a function of the strain invariants. This subroutine can handle and update solution-dependent internal variables and requires that the derivatives of the strain-energy function are defined with respect to the scalar invariants $I_1, I_2, I_3, I_4^{\text{fib}}, I_6^{\text{fib}}, I_4^{\text{smc}}$, which are provided as input. It is called at each integration point during each load increment to calculate the total strain energy Ψ and its first and second derivatives with respect to the invariants $\partial\Psi/\partial I_i$ and $\partial^2\Psi/\partial I_i \partial I_j$ for $i, j = 1, 2, 3, 4^{\text{fib}}, 6^{\text{fib}}, 4^{\text{smc}}$.

Through the input file, a local coordinate system must be set, containing the local directions α^{fib} for the collagen fibres and α^{smc} for the smooth muscle cells.

When defining the material, memory must be allocated for nine solution-dependent state variables, namely the damage driving forces $\beta^{\text{mat}}, \beta^{\text{fib}_4}, \beta^{\text{fib}_6}$, and β^{smc} , and the damage thresholds $\Psi_0^{\text{mat}}, \Psi_0^{\text{fib}_4}, \Psi_0^{\text{fib}_6}$, and Ψ_0^{smc} . The ninth state dependent variable is the relative sliding u_{rs} in the actin-myosin complex, which needs to be stored because of its viscous nature.

The anisotropic, hyperelastic, user-defined material model must be specified with all the material parameters described above, choosing the options ‘formulation = invariant’, ‘local directions = 3’ and ‘type = incompressible’. A conceptual drawback of the UANISOHYPER_INV subroutine is that it does not provide access to the time step of the solution process, which should be known for correct programming of the viscous evolution law described in equation (20). This implies that the exact time step is only known if a fixed time increment is set, by adding the option ‘direct’ to the keyword ‘static’ in the inputfile. Otherwise, only the minimum and maximum allowable time step can be externally prescribed.

3.2 Model problem of cyclic uniaxial tension

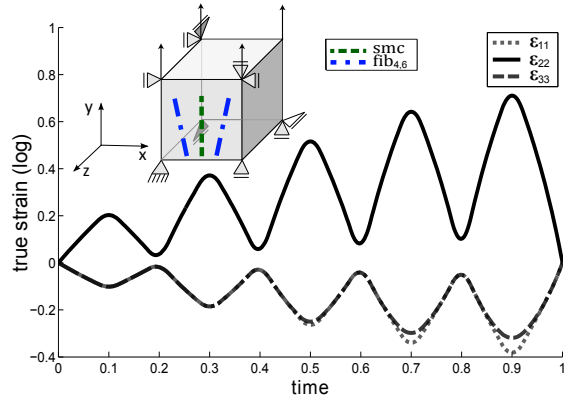


Fig. 1 Strain profile for homogeneous cyclic uniaxial tension. $\epsilon_{11}, \epsilon_{22}$ and ϵ_{33} are the strains in the three principal directions. The lines in the block depict the average direction of the two collagen fibre families and the smooth muscle cells.

The new constitutive model was tested for the simple model problem of cyclic uniaxial tension using a hexahedral C3D8H element. Homogeneous boundary conditions were applied, namely a gradually increasing, sawtooth stretch pattern, as shown in Figure 1. To explore the parameter sensitivity of the model, three different sets of material parameters were compared by altering the smooth muscle cell stiffness μ^{smc} and the damage weighting factor γ^i , see Table 1. All other parameters

Table 1 Parameter sets for cyclic uniaxial tension test in Section 3.2. All other material parameters can be found in Table 2.

Parameter	Variation 1	Variation 2	Variation 3
μ^{smc}	0.0 kPa	0.2 kPa	0.2 kPa
γ^i	0.0(-)	0.0(-)	0.9(-)
$i = \text{mat}, \text{fib}_4, \text{fib}_6, \text{smc}_{\text{pas}}, \text{smc}_{\text{act}}$			

were selected according to the rationale explained in Section 4.2 as shown in Table 2.

As a first benchmark test, the three-constituent damage model was compared to the Abaqus implementation of the standard Holzapfel-Gasser-Ogden model, where the smooth muscle cell stiffness μ^{smc} and the damage weighting factors γ^i were set to zero (variation 1). Both simulations yielded exactly the same results, verifying the correct implementation of the baseline model. Next, different features of the model were gradually added and evaluated for consistency. Figure 2 shows the stress-strain curves for the prescribed loading pattern from Figure 1 for three variations of the new material model. By turning off the smooth muscle contribution μ^{smc} and the damage $\gamma^i = 0$ in variation 1, the model captures the Holzapfel-Gasser-Ogden material by Abaqus as a special case. When the smooth muscle stiffness μ^{smc} is increased to a value of 0.2 MPa in variation 2, the solid green curve is obtained. It shows how, in the fully contracted state, the smooth muscle cells actively contribute to the stiffness. When the damage material parameter γ^i is increased to 0.9 (-) in variation 3, the solid red curve with arrows is obtained, clearly demonstrating the progressive smooth muscle cell degradation. By increasing or decreasing the damage weighting factor γ^i within the range $0 < \gamma^i < 1$, the solid red curve with arrows decreases or increases, respectively, bounded from above and below by the solid green and dashed blue lines.

4 Smooth muscle cell damage through clamping

The three-constituent damage model is put to use to simulate the damage process occurring during the clamping of a rat abdominal artery. To test the realism of the model, the results were compared to actual experiments, more thoroughly described in Famaey et al. [2010], in which the abdominal arteries of rats were clamped up to a defined clamping force. Subsequently, to quantify the degradation of the smooth muscle cells, the contracting capability of the clamped segment was measured in a myograph as explained in Section 4.1. Both experimental processes, i.e., arterial clamping and subsequent myograph testing, were simulated numeri-

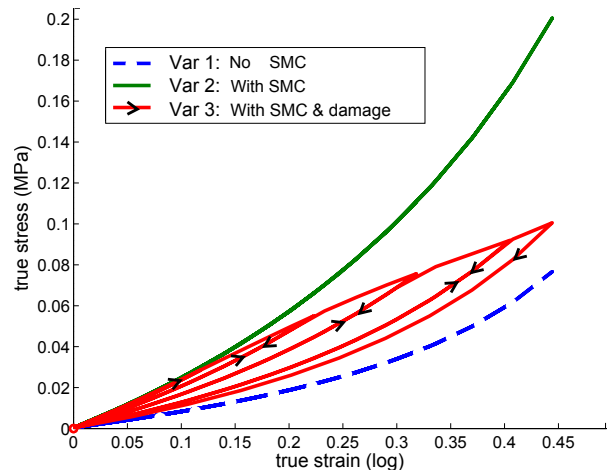


Fig. 2 Stress-strain curve for homogeneous cyclic uniaxial tension test. Curves correspond to healthy smooth muscle (solid green), progressively damaging smooth muscle (solid red with arrows), and no smooth muscle (dashed blue). The prescribed loading profile is shown in Figure 1. The different sets of material parameters, and are summarised in Table 1.

cally using the three-constituent damage model as described in Section 4.2.

4.1 Experimental model

Arterial clamping

In order to correlate the degree of damage to the degree of mechanical loading to which the tissue was previously subjected, loading should be applied in a controllable way. Ideally, loading should be applied *in vivo*, so that the induced damage can be solely attributed to the loading and not to non-physiological *ex vivo* conditions. Since subsequent damage quantification requires excision of tissue, undamaged control segments should also be excised and tested as controls, to rule out damage due to the excision process. To clamp the artery in a controlled way, a hand-held mechanical device, shown in Figure 3, was designed that allows clamping of a rat abdominal artery in an *in vivo* setting to a known force, measured with strain gauges on the clamping arms [Famaey et al., 2010].

Functional damage assessment

One damage quantification method is to compare the degree of functionality of a damaged tissue to that of an intact one. For the specific case of arterial tissue, functionality refers to the vasoregulating capability of the tissue, i.e., the potential of the smooth muscle cells to contract or relax in order to regulate the blood pressure. This vasoregulating capability can be quantified in an experimental setup, known as a ‘myograph’.

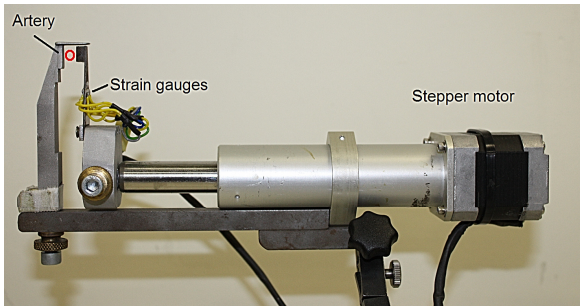


Fig. 3 Mechanical clamping device.

Schematically shown in Figure 4, the myograph consists of a water-jacketed organ chamber in which an excised cylindrical section of an artery can be mounted. Two rods slide into the lumen of the sample, whereby one rod is connected to the base of the setup, and the other to a load cell suspended above the setup, so that isometric tension can be recorded. The height of the load cell can be manually adjusted to set an optimal preload on the sample. The sample is immersed in a Krebs buffer at 37 °C and continuously gassed with a mixture of 95% oxygen and 5% carbon dioxide. After stabilization at the optimal preload level, Phenylephrine (PE) at 10^{-6} M is added to the solution to induce contraction. PE is a contracting agent that acts directly on the smooth muscle cells. Sodium nitroprusside (SNP) (10^{-6} M) induces an endothelium-independent relaxation so consequently an adequate level of SNP-induced relaxation will indicate intactness of the smooth muscle cells [Callera et al., 2000]. Absolute values of relaxation as well as the percentage of relaxation relative to the amount of contraction are recorded and provide a quantitative measure of the damage to the smooth muscle cells when comparing these values to those of an intact sample. More details on the experimental setup can be found in Famaey et al. [2010]. A similar custom-designed device to test active force generation in response to electrical stimulation is reported in Böl et al. [2011].

4.2 Computational model

Arterial clamping

A three dimensional finite element model was built in Abaqus/Standard 6.10-2. Here, an idealised cylindrical geometry was used with an outer radius of 0.58 mm, a wall thickness of 0.14 mm and an initial length of 0.1 mm. For the generation of real patient-specific models,

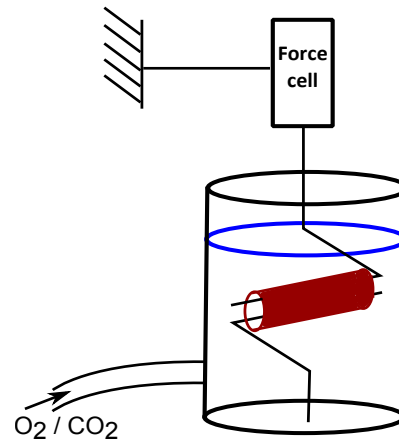


Fig. 4 Custom made functional testing device. Two rods slide into the lumen of the sample, one rod is connected to the base of the setup, the other to a load cell suspended above the setup, so that isometric tension can be recorded. The sample is immersed in water-jacketed organ chamber filled with Krebs buffer.

we refer to Kuhl et al. [2007] or Balzani et al. [2011]. C3D8H elements were assigned to the mesh. The numerical implementation of arterial clamping is subdivided into two steps, (i) the setting of the initial damage level and (ii) the clamping process. Figure 5 shows all steps of the clamping simulation.

In the first part, an opened cylindrical segment with an opening angle of 60° is closed to account for the circumferential residual stresses [Balzani et al., 2007]. Next, the segment is longitudinally stretched by 50%, to account for residual stresses in the longitudinal direction. In the third step, the segment is inflated to an internal pressure of 16 kPa. The material model used in this step is the undamaged three-constituent damage model, however, without accumulation of damage. At the end of the third step, the undamaged elastic strain energy of each of the four constituents is written into a matrix of internal or ‘solution dependent variables’ for each integration point, using Python scripting. These are the initial damage threshold levels Ψ_0^i , described in equations (12), (16) and (23) to be used in step 4.

Step 4 starts with a new input file, in which the state of the artery after the first three steps is imported. By importing, the deformations are included as ‘initial values’ for the model. The solution dependent variables defined above contain the damage threshold levels Ψ_0^i specified as ‘initial conditions’ in the input file. The material model is now updated to enable damage accumulation, $\gamma^i > 0$, and four extra solution dependent variables, representing the β^i described in equations (12), (16)

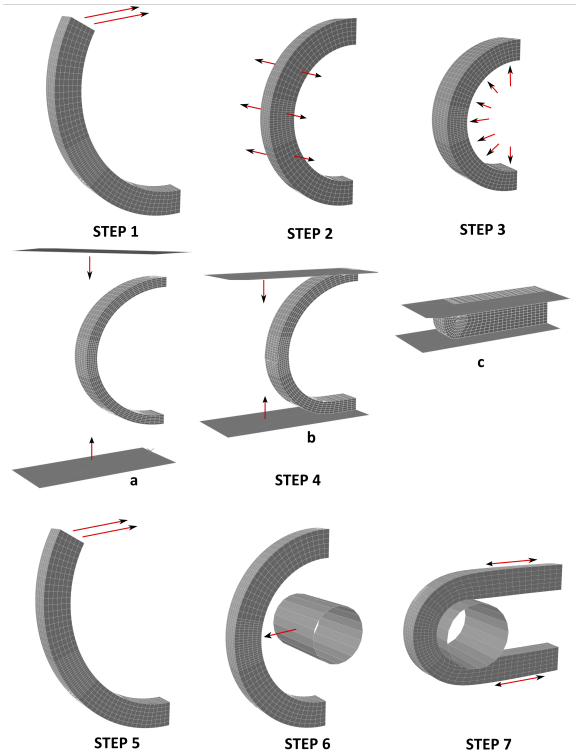


Fig. 5 Schematic overview of the seven steps to represent the loading history of arterial clamping in the FE simulation.

and (23) are added. In addition, two extra parts are added to the assembly of the system, namely an upper and lower clamp, which are gradually moved towards each other during step 4, until a clamping force of 5 mN is reached. A friction coefficient of $\mu^{\text{clamp}} = 0.5$ is used between the clamp and the outer arterial surface. Finally, also the internal pressure boundary conditions are modified to a pulsating pressure between 10 and 16 kPa, that gradually decays to zero when the vessel is completely closed. To keep track of the maximum energy level reached for each constituent at every integration point of the system, the four extra solution dependent variables are updated and stored at each step as internal variables β^i . At the end of the simulation, these solution dependent variables are again written to a matrix using Python scripting to inform the next step.

Functional damage assessment

After clamping, damage has accumulated in the different constituents. For the smooth muscle cells, this amount of damage can be calibrated and validated in a myograph, as explained in Section 4.1. The simulation starts from the same mesh as in step 1 of Section 4.2. This time, however, the initial conditions are specified for the solution dependent variables taking into account the earlier loading history through the internal

variables β^i . The material model is adapted, such that damage due to the energy accumulation of clamping is present, but no further damage is induced. Similar to step 1 of Section 4.2, the segment is closed to form a half cylinder in step 5, thus incorporating the circumferential residual stress. To reproduce the experimental situation, this time, no longitudinal stretch or internal pressure was added. Next, in step 6, a rod is translated radially from inside the section, pulling it until it exerts a certain load, corresponding to the experimentally measured value after complete relaxation due to the addition of SNP. A friction coefficient of $\mu^{\text{rod}} = 0.5$ is used between the rod and the outer arterial surface. Up to the end of step 6, no smooth muscle cell contribution is added in the material model. This is accomplished by multiplying the fractions n_{III} and n_{IV} with a switch function that is set to zero in steps 5 and 6.

After reaching the relaxed state, in the final step, the switch function is smoothly ramped to one, so that the smooth muscle cells reach the completely contracted state. Physiologically, this situation corresponds to the state after the addition of PE. In this step only, because of the time dependence of the evolution law for the relative sliding u_{rs} , the time step of the implicit solution scheme is fixed to $dt = 10^{-5}$. Figure 5 gives a schematic overview of all seven steps of the simulation.

Parameter selection

Table 2 gives an overview over all parameters of the material model. The first set of parameters are related to the extracellular matrix with two embedded fibre families. For the rat abdominal aorta, the main direction of the collagen fibres α^{fib} is set to $\pm 5^\circ$, i.e., it is almost aligned with the circumferential direction, see O’Connell et al. [2008]. The four remaining parameters are set to $\kappa = 0.16$ (-), $k_1 = 32.51$ kPa, $k_2 = 3.05$ (-) and $c = 23.63$ kPa, by using experimental data from extension-inflation tests as described in Famaey et al. [2011]. Alternatively, a parameter set from human arteries can be found in Stålhand [2009].

The next set of parameters are the rate constants of the chemical model defining the fractions n_{III} and n_{IV} in equation (see equation 19). They are chosen according to Hai and Murphy [1988]. These values led to the fractions of $n_{III} = 0.164$ and $n_{IV} = 0.547$, which were used as fixed input values into the mechanical model. Additional parameters are related to the mechanical model of the smooth muscle cell contribution. According to O’Connell et al. [2008], the smooth muscle cells of rat abdominal arteries are oriented circumferentially with $\alpha^{\text{smc}} = 0^\circ$. The parameter μ^{smc} depending on the stiffness of the actin-myosin filament structure and the pa-

parameter κ_c related to the driving force per cross-bridge were both calibrated using the experimental contraction measured in the myograph due to addition of PE for a previously undamaged segment, as described in Section 4.1. The viscous damping constant η was set to 60 MPas, corresponding to the value used in Murtada et al. [2010].

To characterize damage progression appropriately, two parameters need to be calibrated for each constituent, plus two additional ones for the smooth muscle cells, totalling ten parameters. Since the myograph experiment only allows for damage quantification in the smooth muscle cells, with the current setup, no reasonable damage parameters can be defined for the extracellular matrix and the collagen fibres. Additional complementary experiments will be needed for this task, as discussed in Section 5. Accordingly, here, γ^{mat} and γ^{fib} were set to zero, such that m^{mat} and m^{fib} can take any arbitrary value. Secondly, the assumption was made that, during clamping, the smooth muscle cells were completely passive, and thus not contributing to the stiffness. Consequently, no damage could accumulate here, so that $\gamma_{\text{act}}^{\text{smc}}$ could also be set to zero, and $m_{\text{act}}^{\text{smc}}$ to an arbitrary value. The two remaining parameters $\gamma_{\text{pas}}^{\text{smc}}$ and $m_{\text{pas}}^{\text{smc}}$ were then calibrated using the experimental data. For a systematic approach to identify damage material parameters in a heterogeneous setting, the reader is referred to Mahnken and Kuhl [1999].

4.3 Results

The top image in Figure 6a shows the maximum principal stress in an arterial segment in the systolic physiological state. This state defines the damage threshold above which damage is initiated. In the lower image of Figure 6a, the maximum principal stress is shown for the same arterial segment when clamped up to a clamping force of 5 mN. Figure 6b shows the same set of images, this time displaying the elastic strain energy in the matrix material, $\hat{\Psi}^{\text{mat}}$, i.e., the driving force for both isotropic matrix damage d^{mat} and passive smooth muscle cell damage $d_{\text{pas}}^{\text{smc}}$. As shown in the lower image of Figure 6c, the clamping has induced an inhomogeneous damage pattern to the smooth muscle cells. Even when the segment returns to its reference state (top image in Figure 6)c, this damage is irreversible and remains.

Figure 7 shows snapshots of the myograph experiment, with the color code depicting the maximum principal stress. The left graph of Figure 8 shows the force measured in the rods of the myograph as a function of time, for a previously undamaged segment, solid line, and for a segment that was previously clamped at 5

Table 2 Parameters used in the finite element model.

matrix material		
Parameter	Value	Source
c	23.63 kPa	Famaey et al. [2011]
γ^{mat}	0 (-)	Not studied
m^{mat}	1 kPa	Not studied
collagen fibres		
Parameter	Value	Source
α^{fib}	$\pm 5^\circ$	O’Connell et al. [2008]
k_1	32.51 kPa	Famaey et al. [2011]
k_2	3.05 (-)	
κ	0.16 (-)	Not studied
γ^{fib}	0 (-)	
m^{fib}	1 kPa	Not studied
smooth muscle cells - chemical rate constants		
Parameter	Value	Source
κ_1, κ_6	0.14 s^{-1}	Hai and Murphy [1988]
κ_2, κ_5	0.5 s^{-1}	
$\kappa_3, 4\kappa_4$	0.44 s^{-1}	
κ_7	0.01 s^{-1}	
smooth muscle cells - mechanical constants		
Parameter	Value	Source
μ^{smc}	0.25 MPa	Fitted to experiments
κ_c	0.93 MPa	Fitted to experiments
η	60 MPa s	Murtada et al. [2010]
α^{smc}	0°	O’Connell et al. [2008]
$\gamma_{\text{act}}^{\text{smc}}$	0 (-)	Not studied
$m_{\text{act}}^{\text{smc}}$	1 kPa	Not studied
$\gamma_{\text{pas}}^{\text{smc}}$	0.9 (-)	Fitted to experiments
$m_{\text{pas}}^{\text{smc}}$	0.03 MPa	Fitted to experiments

mN, dashed. The letters along the curve correspond to the stages shown in Figure 7. The first section of the graph corresponds to step 6 of the simulation, i.e., the pulling of the rod to the passive state. After 2 seconds, the smooth muscle cells are activated, corresponding to step 7.

The right graph of Figure 8 shows the force measured in the rod for a segment that was previously clamped with the device described in Section 4.1 to a level of 5 mN, normalised to the width of the numerical model, and for a segment that was undamaged. The force in the rod was also normalised to the width of the numerical model. Again, in the first section of the graph, the rod is gradually pulled to reach the passive preload state. At the point indicated with the arrow, PE is added to the Krebs solution, triggering the activation of the smooth muscle cells. Note that the time scales in the two graphs do not agree. To calibrate the model appropriately, an additional time parameter would have to be included into the model. Here, however, we were only interested in the end result of the curve, rather than in calibrating the model to real physical times.

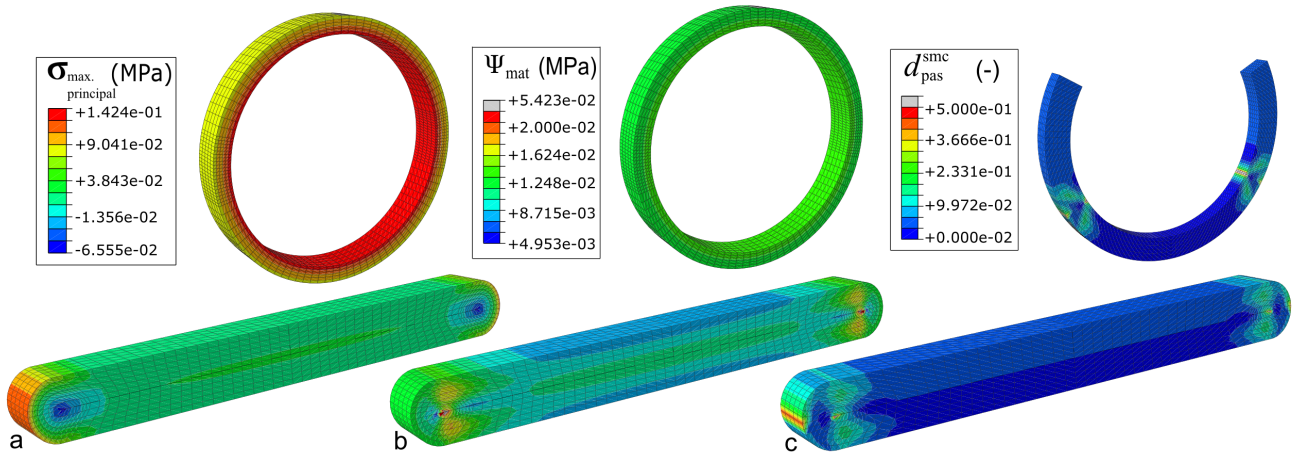


Fig. 6 (a). Maximum principal stress in an arterial segment in systolic physiological state (top image), and when clamped up to a clamping force of 5 mN (lower image). (b). Strain energy in the same two segments as in (a). (c). Damage variable d_{pas}^{smc} in the same arterial segment as in Figure 6, when clamped up to a clamping force of 5 mN (lower image). This damage remains, even when the segment returns to its reference state (top image).

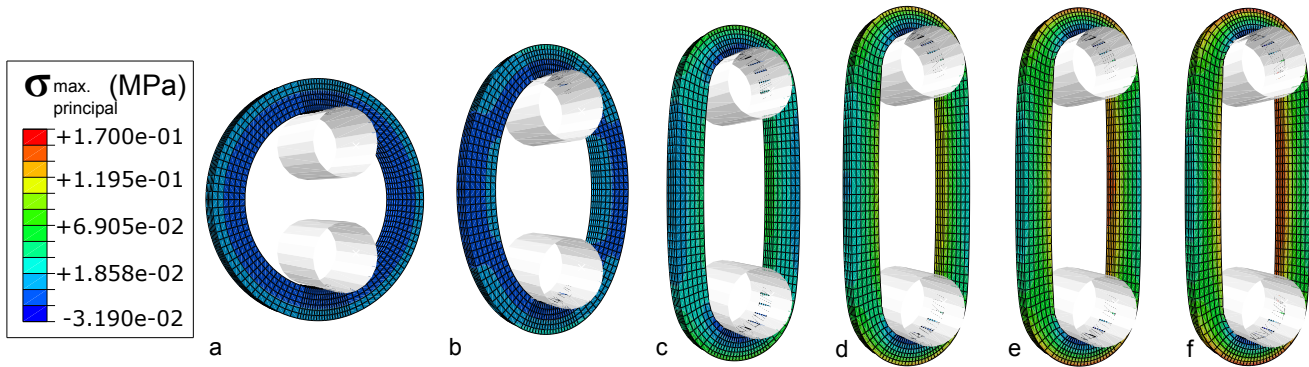


Fig. 7 Different stages of the myograph experiment, with the color code depicting the maximum principal stress. In stages a,b and c, the rods are being pulled to the preload force (step 6 of the numerical simulation). In stages d, e and f, the rods remain in position and the smooth muscle cells are activated (step 7 of the numerical simulation).

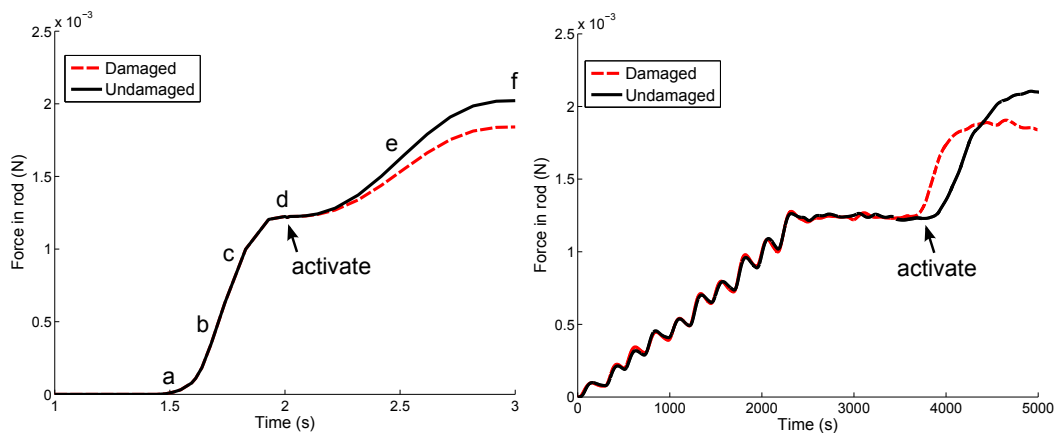


Fig. 8 The left graph shows the force measured in the rod of the myograph as a function of time, for a previously undamaged segment (solid line) and for a segment that was previously clamped at 5 mN (dashed). The letters along the curve correspond to the snapshots shown in Figure 7. The right graph shows the force measured in the rod during an experiment, for a segment that was previously clamped with the device described in Section 4.1 to a level of 5 mN and for a segment that was undamaged, both normalised to the width of the numerical model.

5 Discussion

In this paper, a three-constituent damage constitutive model was proposed to simulate the damage process in arterial tissue. After testing the model in a homogeneous model problem under cyclic uniaxial tension, it was used in a finite element simulation for the clamping of an artery and the subsequent damage evaluation in a myograph. The model enables the analysis of the inhomogeneous damage profile in the artery due to loading, quantitatively showing which constituents and which sections are overloaded, compared to the physiological state. In response to overload, driven by the free energy, anisotropic damage develops in the smooth muscle cells. The three-constituent damage model and numerical simulation provide a useful tool to explore safe loading of arterial tissue. Being able to reliably predict loading regimes which initiate tissue damage is important in view of robotic surgery, which lacks the natural feedback of human touch, by which the experienced surgeon today guarantees safe tissue loading.

The material model described in Section 2 introduces a large set of parameters, which need to be experimentally defined for each tissue type. Extensive experimental data from a range of different experiments is required to correctly identify all parameters. Section 4.2 comments on the rationale behind the parameter selection for this study. The goal of this study was to demonstrate the feasibility of the proposed model and to illustrate a conceptual methodology for the damage characterization in smooth muscle cells. Accordingly, less emphasis was placed on the exact parameter identification for the other model parameters. As explained in section 2.2, four damage processes can be captured by the model, one for each constituent. Each damage process is assumed to be driven by the individual free energy of that constituent. For smooth muscle cells, passive damage is also affected by the energy in the matrix constituent. Here, we focus in particular on this last passive part of damage, assuming that smooth muscle cells are inactive during the real clamping process. The damage parameters were chosen to correspond to the results of an *ex vivo* experiment. In the future, further experiments will be performed with different clamping force levels to calibrate the model for a wider loading range. To enable numerical comparison with higher clamping force levels, it might become relevant to remesh the the clamped segment to avoid excessive element distortion. However, remeshing would require the mapping of the solution, both from the node points and from the integration points, onto the new mesh, a feature currently still lacking for anisotropic materials in Abaqus 6.10.

In order to define the damage parameters for all constituents, different experiments are required that enable the extraction of this specific information. A possible way to study damage to the collagen fibres in tension is to acquire microscopic images of the tissue at different stages in the stretching process and assess the images for collagen rupture. In fact, the extension-inflation tests that were used here to identify the undamaged baseline parameters of the Holzapfel model most probably already induced damage to the matrix and the collagen fibres in the higher pressure regimes. Ideally, damage to the matrix and collagen constituents should therefore be included in the parameter identification process of the extension-inflation tests.

Although the three-constituent damage model already

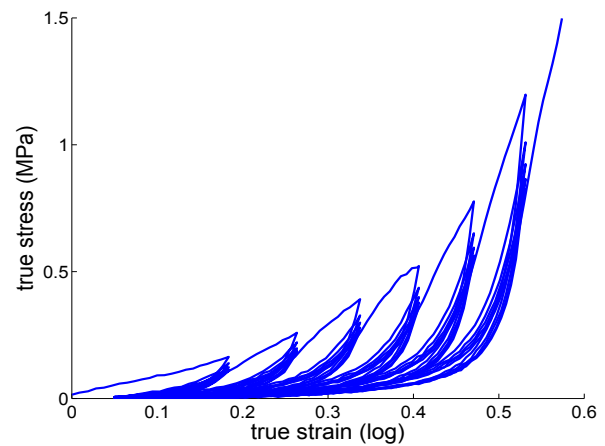


Fig. 9 Uniaxial tensile test on a circumferentially oriented strip of a sheep carotid artery. The loading profile was such that each strain level was cycled five times, for six increasing levels of strain.

captures a number of typical features of cardiovascular tissue, some features are still not included, or simplified. When qualitatively comparing the homogeneous cyclic tension test described in Section 3.2 to the results of a uniaxial tensile test on a sheep carotid artery, shown in Figure 9, aspects such as nonlinearity and discontinuous softening are nicely represented. However, in the tensile test on the sheep carotid artery, cycling up to a certain strain level was performed five times before the next strain level was reached, and clearly softening does continue in these cycles, even though the maximum energy level, the parameter β in our model, is not increased. This continuous damage behaviour was not captured with the damage model used here. Moreover, the damage variables introduced in this model mainly capture acute effects, while chronic effects such as repair and/or remodelling have not been considered for the time being. These effects should be investigated,

keeping in mind the trade-off between realism of the model and its usability. The correct identification of the material parameters becomes obviously more challenging the more effects are incorporated in the model.

The ultimate goal of this research project is to minimize tissue trauma during surgery, for which damage thresholds need to be identified. These thresholds should be defined in close collaboration with surgeons and biomedical researchers, experimentally assessing the level of damage due to loading and defining which damage levels are still acceptable, taking into account long-term effects of damage accumulation but also self healing. These critical damage levels can then be correlated to the internal damage variables d . Once the damage variable of a constituent has reached a certain level, the damage is set to be unacceptable, and robotic loading should be stopped automatically. Future research will therefore also be directed towards algorithm speed-up, e.g., through parallelised implementation in the GPU with NVIDIA Compute Unified Device Architecture.

Predictive computational modeling of tolerable damage thresholds is clinically relevant in two ways: on the one hand, in the short term, the proposed model can be used as a simulation tool to optimize surgical tools, for example, to improve clamp design to minimize tissue damage. On the other hand, in the long term, the proposed model could enable the prediction of surgically-induced damage evolution in real-time. This would allow to impose loading thresholds on surgical instruments during an operation in a robotic teleoperation setting.

Acknowledgements This work was supported by a PhD grant from the Institute for the Promotion of Innovation through Science and Technology in Flanders (I.W.T.-Vlaanderen), a travel grant from the Research Foundation - Flanders, a travel grant from the Prof. R. Snoeys Foundation and a Fulbright scholarship.

References

- D. Balzani, J. Schröder, and D. Gross. Simulation of discontinuous damage incorporating residual stresses in circumferentially overstretched atherosclerotic arteries. *Acta Biomater*, 2(6):609–618, Nov 2006. doi: 10.1016/j.actbio.2006.06.005.
- D. Balzani, S. J., and G. D. Numerical simulation of residual stresses in arterial walls. *Comp Mat Sci*, 39: 117–123, 2007.
- D. Balzani, D. Böse, D. Brads, R. Erbel, A. Klawonn, O. Reinbach, and S. J. Parallel simulation of patient-specific atherosclerotic arteries for the enhancement of intravascular ultrasound diagnosis. *Eng Comp*, in press, 2011.
- G. W. Barone, J. M. Conerly, P. C. Farley, T. L. Flanagan, and I. L. Kron. Assessing clamp-related vascular injuries by measurement of associated vascular dysfunction. *Surgery*, 105(4):465–471, Apr 1989.
- M. Böl, O. J. Abilez, A. N. Assar, C. K. Zarins, and E. Kuhl. In vitro / in silico characterization of active and passive stresses in cardiac muscle. *Int J Multi-scale Comp Eng*, in press, 2011.
- G. E. Callera, W. A. Varanda, and L. M. Bendhack. Impaired relaxation to acetylcholine in 2k-1c hypertensive rat aortas involves changes in membrane hyperpolarization instead of an abnormal contribution of endothelial factors. *Gen Pharmacol*, 34(6):379–389, Jun 2000.
- B. Calvo, M. Pena, M. Martinez, and M. Doblaré. An uncoupled directional damage model for fibred biological soft tissues. formulation and computational aspects. *Int J Num Meth Eng*, 69:20362057, 2007.
- S. De, J. Rosen, A. Dagan, H. B., P. Swanson, and M. Sinanan. Assessment of tissue damage due to mechanical stresses. *Int J Robotics Res*, 26:1159–1171, 20–22 Feb. 2007. doi: 10.1109/BIOROB.2006.1639192.
- N. Famaey and J. Vander Sloten. Soft tissue modelling for applications in virtual surgery and surgical robotics. *Comp Meth Biomech Biomed Eng*, 11(4): 351–366, Aug 2008.
- N. Famaey, E. Verbeken, S. Vinckier, B. Willaert, P. Herijgers, and J. Vander Sloten. In vivo soft tissue damage assessment for applications in surgery. *Med Eng Phys*, 32:437–443, 2010.
- N. Famaey, J. Vander Sloten, and G. A. Holzapfel. Experimental study and numerical analysis of arterial clamping. *J Mech Behav Biomed Mat*, page Submitted, 2011.
- Y. C. Fung. Mathematical representation of the mechanical properties of the heart muscle. *J Biomech*, 3(4):381–404, Jul 1970.
- T. C. Gasser, R. W. Ogden, and G. A. Holzapfel. Hyperelastic modelling of arterial layers with distributed collagen fibre orientations. *J Royal Soc Interface*, 3(6):15–35, Feb 2006.
- S. Gestrelus and P. Borgström. A dynamic model of smooth muscle contraction. *Biophys J*, 50(1):157–169, Jul 1986. doi: 10.1016/S0006-3495(86)83448-8. URL [http://dx.doi.org/10.1016/S0006-3495\(86\)83448-8](http://dx.doi.org/10.1016/S0006-3495(86)83448-8).
- R. L. Gleason, S. P. Gray, E. Wilson, and J. D. Humphrey. A multiaxial computer-controlled organ culture and biomechanical device for mouse carotid arteries. *J Biomech Eng*, 126(6):787–795, Dec 2004.

- S. Göktepe and E. Kuhl. Electromechanics of the heart - a unified approach to the strongly coupled excitation-contraction problem. *Comp Mech*, 45:227–243, 2010.
- S. Göktepe, S. N. S. Acharya, J. Wong, and E. Kuhl. Computational modeling of passive myocardium. *Int J Num Meth Biomed Eng*, 27:1–12, 2011.
- V. Gupta, N. P. Reddy, and P. Batur. Forces in laparoscopic surgical tools. *Presence*, 6:218–228, 1997.
- C. M. Hai and R. A. Murphy. Cross-bridge phosphorylation and regulation of latch state in smooth muscle. *Am J Physiol*, 254(1 Pt 1):C99–106, Jan 1988.
- A. Hill. The heat of shortening and the dynamic constants of muscle. *Proc Royal Soc London B*, 126:136195, 1938.
- J. Hokanson and S. Yazdani. A constitutive model of the artery with damage. *Mech Res Comm*, 24 (2):pp. 151–159, 1997.
- G. A. Holzapfel and R. W. Ogden. Modelling the layer-specific three-dimensional residual stresses in arteries, with an application to the human aorta. *J Royal Soc Interface*, 7:787–799, 2010.
- G. A. Holzapfel, T. C. Gasser, and R. W. Ogden. A new constitutive framework for arterial wall mechanics and a comparative study of material models. *J Elast*, 61:1–48, 2000.
- C. Hsi, H. Cuenoud, B. R. Soller, H. Kim, J. Favreau, T. J. V. Salm, and J. M. Moran. Experimental coronary artery occlusion: relevance to off-pump cardiac surgery. *Asian Cardiovasc Thor Ann*, 10(4):293–297, Dec 2002.
- A. Itoh, G. Krishnamurthy, J. Swanson, D. Ennis, W. Bothe, E. Kuhl, M. Karlsson, L. Davis, D. C. Miller, and N. B. Ingels. Active stiffening of mitral valve leaflets in the beating heart. *Am J Physiol Heart Circ Physiol*, 296:1766–1773, 2009.
- M. Kroon. A constitutive model for smooth muscle including active tone and passive viscoelastic behaviour. *Math Med Biol*, 27(2):129–155, Jun 2010. doi: 10.1093/imammb/dqp017. URL <http://dx.doi.org/10.1093/imammb/dqp017>.
- E. Kuhl, R. Maas, G. Himpel, and A. Menzel. Computational modeling of arterial wall growth: Attempts towards patient specific simulations based on computer tomography. *Biomech Mod Mechanobio*, 6:321–331, 2007.
- Y. S. Kwok, J. Hou, E. A. Jonckheere, and S. Hayall. A robot with improved absolute positioning accuracy for ct guided stereotactic brain surgery. *IEEE Trans Biomed Eng*, 35:153–161, 1988.
- R. Mahnken and E. Kuhl. Parameter identification of gradient enhanced damage models with the finite element method. *Eur J Mech/A: Solids*, 18:819–835, 1999.
- J. V. Manchio, J. Gu, L. Romar, J. Brown, J. Gammie, R. N. Pierson, B. Griffith, and R. S. Poston. Disruption of graft endothelium correlates with early failure after off-pump coronary artery bypass surgery. *Ann Thorac Surg*, 79(6):1991–1998, Jun 2005.
- C. Miehe. Discontinuous and continuous damage evolution in ogden-type large-strain elastic materials. *Euro J Mech A/Solids*, 14:697–720, 1995.
- F. W. Mohr, V. Falk, A. Diegeler, T. Walther, J. F. Gummert, J. Bucarius, S. Jacobs, and R. Autschbach. Computer-enhanced robotic cardiac surgery: Experience in 148 patients. *J Thorac Cardiovasc Surg*, 121:842–853, 2001.
- S.-I. Murtada, M. Kroon, and G. A. Holzapfel. A calcium-driven mechanochemical model for prediction of force generation in smooth muscle. *Biomech Model Mechanobiol*, 9(6):749–762, Dec 2010. doi: 10.1007/s10237-010-0211-0.
- M. K. O’Connell, S. Murthy, S. Phan, C. Xu, J. Buchanan, R. Spilker, R. L. Dalman, C. K. Zarins, W. Denk, and C. A. Taylor. The three-dimensional micro- and nanostructure of the aortic medial lamellar unit measured using 3d confocal and electron microscopy imaging. *Matrix Biol*, 27(3):171–181, Apr 2008. doi: 10.1016/j.matbio.2007.10.008.
- R. W. Ogden and D. G. Roxburgh. A pseudo-elastic model for the mullins effect in filled rubber. *Proc Royal Soc A*, 455:28612877, 1999.
- E. Pena, V. Alastrué, A. Laborda, M. Matrínez, and M. Doblaré. A constitutive formulation of vascular tissue mechanics including viscoelasticity and softening behaviour. *J Biomech*, 43:984–989, 2010.
- M. K. Rausch, A. Dam, S. Göktepe, O. J. Abilez, and E. Kuhl. Computational modeling of growth: Systemic and pulmonary hypertension in the heart. *Biomech Mod Mechanobio*, in press: doi:10.1007/s10237-010-0275-x, 2011.
- J. A. G. Rhodin. Architecture of the vessel wall. In R. M. Berne, editor, *Handbook of Physiology, Section 2, Volume 2*. Am. Physiol. Soc., Bethesda, 1979.
- J. F. Rodríguez, F. Cacho, J. A. Bea, and M. Doblaré. A stochastic-structurally based three dimensional finite-strain damage model for fibrous soft tissue. *J Mech Phys Solids*, 54(4):864 – 886, 2006. ISSN 0022-5096. doi: 10.1016/j.jmps.2005.10.005.
- M. S. Sacks and W. Sun. Multiaxial mechanical behavior of biological materials. *Annu Rev Biomed Eng*, 5:251–284, 2003. doi: 10.1146/annurev.bioeng.5.011303.120714.
- A. Schmitz and M. Böl. On a phenomenological model for active smooth muscle contraction. *J Biomech*, 44:2090–2095, 2011.

- A. J. Schriefl, G. Zeindlinger, D. M. Pierce, P. Regitnig, and G. A. Holzapfel. Determination of the layer-specific distributed collagen fiber orientations in human thoracic and abdominal aortas and common iliac arteries. -, Submitted:–, 2011.
- J. Simo and J. Ju. Strain- and stress-based continuum damage models. *Int J Solids Struct*, 23:821–840, 1987.
- J. Stålhand. Determination of human arterial wall parameters from clinical data. *Biomech Model Mechanobio*, 8, 2009.
- J. Stålhand, A. Klarbring, and G. A. Holzapfel. Smooth muscle contraction: mechanochemical formulation for homogeneous finite strains. *Prog Biophys Mol Biol*, 96(1-3):465–481, 2008. doi: 10.1016/j.pbiomolbio.2007.07.025.
- J. Stålhand, A. Klarbring, and G. A. Holzapfel. A mechanochemical 3d continuum model for smooth muscle contraction under finite strains. *J Theor Biol*, 268(1):120–130, Jan 2011. doi: 10.1016/j.jtbi.2010.10.008.
- A. Tsamis, W. Bothe, J. P. Kvitting, J. C. Swanson, D. C. Miller, and E. Kuhl. Active contraction of cardiac muscle: In vivo characterization of mechanical activation sequences in the beating heart. *J Mech Behavior Biomed Mat*, 4:1167–1176, 2011.
- R. P. Vito and S. A. Dixon. Blood vessel constitutive models-1995-2002. *Annu Rev Biomed Eng*, 5:413–439, 2003. doi: 10.1146/annurev.bioeng.5.011303.120719.
- J. Yang, J. W. Clark, Jr, R. M. Bryan, and C. Robertson. The myogenic response in isolated rat cerebrovascular arteries: smooth muscle cell model. *Med Eng Phys*, 25(8):691–709, Oct 2003.
- M. A. Zulliger, A. Rachev, and N. Stergiopoulos. A constitutive formulation of arterial mechanics including vascular smooth muscle tone. *Am J Physiol Heart Circ Physiol*, 287(3):H1335–H1343, Sep 2004. doi: 10.1152/ajpheart.00094.2004.